Optimisation of the Experimental Conditions for the Smoke Wire Technique in a Boundary Layer Wind Tunnel

A. R. P. Yusrizal[1], N. A. Rahmat[1†], K. K. Abdullah[1], N. A. Zolpakar[1], A. F. Sharol[1] and I. A. Ishak[2]

[1] *Faculty of Mechanical and Automotive Engineering Technology, Universiti Malaysia Pahang As-Sultan Abdullah (UMPSA), Malaysia*
[2] *Faculty of Engineering Technology, Universiti Tun Hussein Onn Malaysia (UTHM), Malaysia*

†*Corresponding Author Email: izzatulatikha@umpsa.edu.my*

ABSTRACT

Optimal experimental conditions, namely the nozzle size, wire diameter, power value, and wind speed, for a smoke wire technique (SWT) with a control dripping valve (CDV) and tensioner system were proposed to ensure dense, straight, and continuous streaklines for flow visualisation experiments. The investigation was conducted using a single heated nichrome wire in a small-scale boundary layer wind tunnel (BLWT) constructed at Universiti Malaysia Pahang As-Sultan Abdullah, Malaysia. Through the CDV, the water-based solution is automatically replenished to the heated single nichrome while maintaining a consistent wire strain with the aid of a specifically designed tensioner system. A simple shape, a surface-mounted finite circular cylinder, was utilised as the rigid body to observe the flow pattern during the experiment, which was verified with findings from previous literature. A high-speed digital camera, the MEMRECAM HX-7s system, was used to record instantaneous images of the streaklines. Clear images of dense, straight, and continuous smoke lines were captured at a free-stream velocity of 1.5 m/s using a 0.5 mm nichrome wire diameter, a 0.6 mm nozzle diameter, and 35 W power conditions.

1. INTRODUCTION

Generally, research topics on the flow around obstacles or buildings in fluid dynamics, and their aerodynamic interaction with the urban boundary layer, are conducted using a single concentrated approach, i.e., scaled-model boundary layer wind tunnel (BLWT) experiments (Niemann, 1993; Barlas et al., 2016; Wang et al., 2017). The BLWT differs from an aeronautical or aerodynamic wind tunnel (WT), which is typically employed in designing aeroplanes or automobiles (Isyumov, 1967; Rahmat et al., 2023a). BLWTs are typically employed to replicate a quasi-atmospheric boundary layer (quasi-ABL), facilitating reactions that are anticipated from natural wind conditions. However, an aeronautical or aerodynamic WT could be converted into a BLWT if the test section length is extended to between 15 and 30 m (Cermak et al., 1995). Alternatively, a small-scale BLWT with a shorter test section can be developed using graded blockage grids of rods (Cook, 1975), slats, and passive devices, such as barriers (Hohman et al., 2015), spires (Rahmat et al., 2018), and rough walls (Rahmat et al., 2016). These are installed in the upwind position of the WT to simulate and enhance the quasi-ABL (Cook, 1975).

The production of a quasi-ABL enables the use of a BLWT to examine the impact of wind on man-made structures (Niemann, 1993; Fu et al., 2008) and pedestrians (Fitriady et al., 2022; Fitriady et al., 2023a, 2023b, 2023c, 2023d).

Experiments to examine the flow structure around bodies or buildings using scaled model BLWTs are a widespread practice in many engineering, physics, and meteorology disciplines. The measurement method for these experiments can be diverse, using either two-(quantitative) or three-dimensional (qualitative) approaches. The hot wire anemometer is widely utilised in two-dimensional measurement techniques (Rahmat et al., 2016, 2018; Vikneshvaran et al., 2020; Fitriady et al., 2023b; Hadi Wijaya et al., 2024). Meanwhile, Particle Image Velocimetry (PIV), Laser Doppler Anemometer/Velocimetry (LDA/LDV), and the Smoke Wire Technique (SWT) are frequently employed in three-dimensional measurement techniques. However, the SWT is a more convenient approach in flow visualisation experiments as it is more cost-effective and flexible to construct in any institution, compared to the former two methods. The SWT produces thin strands of smoke when an electric current heats a coated wire. The current

evaporates a wire-heated glycol-based solution (Yarusevych et al., 2009), a water-based solution (Trinder & Jabbal, 2013; Rahmat et al., 2023a, 2023b), or paraffin oil (Yarusevych et al., 2009; Gao & Liu, 2018). This process allows very fine smoke to be injected into the flow area, resulting in streaks of smoke being emitted into the air stream, which creates a pattern resembling streaks and imparts a streaky appearance to the flow. This approach facilitates the integration of extremely thin smoke streamlines into the flow field.

A variety of smoke liquids have been employed to achieve a clear representation of flow visualisation. The most commonly used types of smoke are vaporised substances, including light oil, kerosene, glycerin, and various commercial smoke liquids. The wire should be coated uniformly with oil to ensure that smoke is generated consistently along its entire length. The coating can be applied through the gravity feed method or directly with brushes. Although the gravity feed technique offers several advantages, such as straightforward installation, its effectiveness may not match that of the manual coating process. The hand-coating procedure allows control over the thickness of oil applied to the wire. Unfortunately, this method is labour-intensive and presents various challenges. However, it is effective for obtaining a result unaffected by the varying coating thicknesses of oil. Compared to the smoke generator, this method has a lower overall implementation cost. Nonetheless, the challenge of this method is that it requires the right kind of oil or solution, metal wire, and a sufficient supply of power to obtain straight, continuous, and dense streaklines. Another key factor in the SWT is the wire material, which typically uses nichrome, stainless steel, and tungsten (Batill & Mueller, 1981; Azizi, 2012). These materials can resist heat, allowing them to bring the oil up to boiling point, at which smoke will be produced.

Since the beginning of WTs, the SWT has been utilised as a method for flow visualisation. The practice has a historical foundation extending over several decades, as reported by Settles (1986), which delineates the smoke-wire approach as a classic tracer technique. In this context, it pertains to the process of generating fine aerosol filaments by applying heat to a wire coated with oil. While primarily utilised in wind turbines functioning at low speeds (Schneider, 2003), this technology has also been applied in wind turbines operating at transonic speeds (Kumaraswamy et al., 2014). In applications that necessitate moderate speeds, utilising a wire with a smaller diameter is advantageous due to its ability to produce a more concentrated smoke output. A larger diameter is more appropriate for higher speeds due to the increased surface area, which facilitates a higher smoking rate. Furthermore, considering that the wires are typically extended, they can sustain the necessary tension at elevated temperatures. The maximum velocity in a WT is reported to be 6.096 m/s (Barlow et al., 1999). Due to its importance in avoiding the wake flow emerging from the wire itself and disturbing the main flow, it is also recommended that the Reynolds numbers be lower than 2000 to reduce the flow disruption (Barlow et al., 1999).

The literature on the SWT has discussed and addressed several drawbacks. The first was discovered by Wu (1992), who found that the smoke wire induced the airflow to establish a fixed vortex pair at an increased velocity. Upon increasing the wind speed to 14.27 m/s, the wire exhibited characteristics akin to a circular cylinder, resulting in the transition of the unseparated flow into a stable vortex pair. The authors were able to prevent this phenomenon by limiting the speed of their WT to 3.96 m/s. They also utilised a single wire, which resulted in disseminated smoke intensity. Second, a manual dripping system (Ismail & Kamaruddin, 2020) easily burns wire due to excess power (Gao & Liu, 2018), leading to blurry instantaneous images (Liu et al., 2013).

The utilisation of a capacitor as the power source was introduced as an advancement of the methodology in a 2018 study by Gao and Liu (2018). Instead of being heated for an extended period continuously, the wires were heated in brief bursts. The authors utilised a microcontroller in conjunction with the capacitor to set the camera timing so that it would take the picture at the appropriate moment. Recently, Rahmat et al. (2023a, 2023b) constructed an enhanced SWT with a dripping system that was fully automated and utilised 10 smoke wires to increase the smoke intensity. However, inadequate drainage of excess liquid from the dripping part led to liquid overflow, causing corrosion inside the WT. In addition, due to a poor tensioner system, the 10 smoke wires experienced a noticeable expansion when heated, distorting them and causing them to become warped. Due to this problem, the generated smoke was not produced to the desired trajectory.

The smoke quality produced, along with the quality of the captured photographs and videos, has been enhanced through the implementation of various additional methods. In 1988, Mathur et al. (1988) published their findings on creating coloured smoke using liquid paraffin coloured with wax-based pigments. In 2006, Dol et al. (2006) conducted experiments on alternative smoke fluids as substitutes for paraffin oil and explored alternative wire configurations using nichrome wire instead of stainless-steel wires. A notable improvement in the overall quality of the produced smoke was reported. The literature concerning the SWT primarily emphasises the importance of the photography technique. Additionally, Wu (1992).reported that a substantial amount of light was necessary to achieve an improved photograph of the smoke movement. This was achieved using two lights, providing a combined output of 1000 W.

It is essential to utilise a high shutter speed to accurately capture the movement of smoke in photographs. Gao and Liu (2018) employed a shutter speed of 1/200 s in their experiment, while Wu (1992) utilised a shutter speed of 1/1000 s. In the context of video recording, a high-speed recording technique was employed, specifically capturing the smoke flow at a rate of 1000 frames per s(Liu et al., 2013). Besides the strategy that incorporates smoke wires, various additional methods have been employed. Soria et al. (1990) employed a cinematographic technique referred to as the silhouette.

This method entails the strategic placement of semi-silvered mirrors at a 45-degree angle relative to the camera, which facilitates the reflection of light to create a shadow effect on the background. The camera captures an image of the silhouette of the smoke instead of the smoke itself. Conversely, Serrano-Aguilera et al. (2016) employed a laser sheet to enhance the visibility of a layer within the smoke flow. In addition to the WT, the smoke wire method has been utilised in various contexts, including the placement of a smoke wire behind a jet to visualise the flow structure over different surfaces (Cornaro et al., 1999) and the positioning of a smoke wire beneath flapping mechanical insect wings to examine the airflow pattern generated by the wings (Liu et al., 2013). The procedure is conducted in an isolation chamber to mitigate the risk of contamination from external air sources.

Considering the existing limitations, this work aimed to develop an improved smoke wire technique featuring an automated control dripping valve and a tensioner wire system. The objective was to achieve intense, straight, and thick streaklines within a specially designed qualitative small-scale BLWT. This paper discusses the optimal conditions of the smoke wire technique, including its nozzle size, wire diameter, power value, and wind speed.

2. EXPERIMENTAL DETAILS

2.1. Small-scale BLWT

An open-loop BLWT has been established at Universiti Malaysia Pahang Al-Sultan Abdullah (UMPSA) to facilitate qualitative flow visualisation experiments. This open-loop BLWT is an upgraded version of a previous tunnel (Abdullah et al., 2022; Rahmat et al., 2023b). The WT is comprised of three primary sections: the contraction, the test section, and the diffuser, as illustrated in Fig. 1. The flow straightener of the WT features a honeycomb structure characterised by a length-to-diameter (L/D) ratio of 10 (Kulkarni et al., 2011), succeeded by three meshes. The open area ratios (β) of the meshes must exceed 0.54 (Bradshaw, 1965; Rosminahar et al. 2024). Therefore, the present work employed meshes with β values of 0.577, 0.631, and 0.645 (Welsh, 2013) in the order from upstream to downstream of the flow straightener section. The spanwise variation of the mean flow at the exit of the upwind contraction section was relatively high, with a relative standard deviation of velocity of approximately 4%, measured at a height of 30 mm from the tunnel floor. This variation was attributed to the inherent effects of the contraction section and the fan. To mitigate this, a flat plate was installed parallel to the tunnel floor at a height of 0.07 m to regenerate a new wall boundary layer. As a result, the relative standard deviation of the velocity at 30 mm above the flat plate was improved to 0.9%. The contraction section utilised a contraction ratio of 9, as indicated by prior studies (Li & Li, 2019; Kareem et al., 2021; Mehta, 2021) and it was designed using a bicubic curve to define the curvature (Yi et al., 2021), as depicted in Fig. 1(a).

The test section features a cross-section measuring 300 mm by 300 mm and a length of 1000 mm,
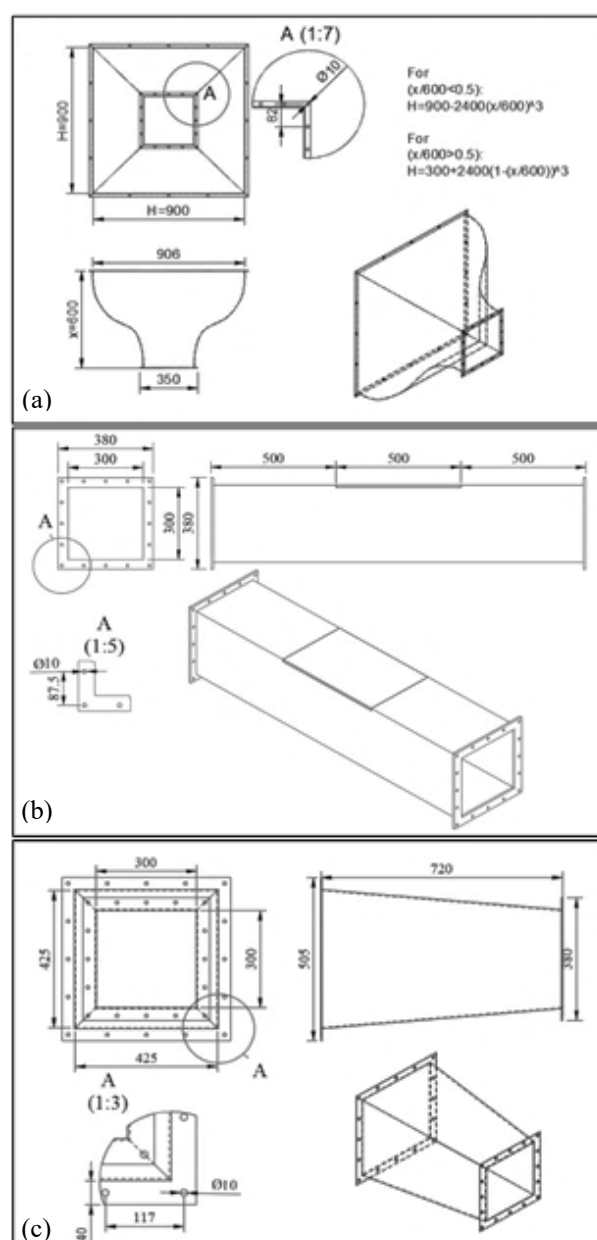

Fig. 1 Schematic figure for a) contraction, b) test section, and c) diffuser of the BLWT

as illustrated in Fig. 1(b). The extended length of the test section facilitates the development of a deep quasi-ABL. The diffuser is utilised in the WT to reduce the airflow velocity as it exits the test section, while concurrently increasing its pressure at an open area ratio of 2 and a diffuser angle of 5° (Mehta & Bradshaw, 1979), as illustrated in Fig. 1(c). Figs. 2(a) and (b) present the schematic diagram, including the dimensions, of the complete assembly of the BLWT, along with an image depicting the fabrication of the small-scale BLWT.

2.2. Smoke Wire Technique

The SWT used in this study comprises three primary components: a CDV, a tensioning system, and a power supply source (Rahmat et al., 2023b). Figure 3 presents a schematic diagram of the CDV with its 11 openings, i.e., holes to connect wires from the CDV to the tank in
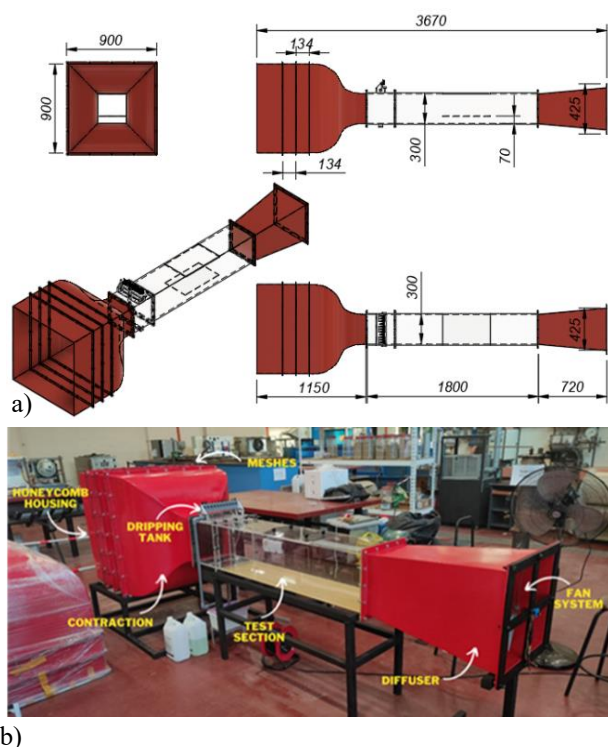
a)

b)

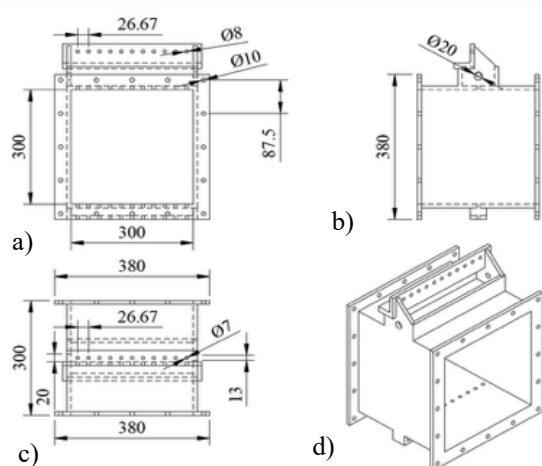**Fig. 2 a) schematic diagram and b) actual picture of the BLWT**

Fig. 3 Schematic diagram of the full setup of CDV with the tensional system for a) front view, b) side view, c) top view, and d) isometric view

position. All three components were developed to identify the optimal SWT conditions to achieve dense, straight, and continuous streaklines using a single heated nichrome wire in the experimental setup. In future studies, 11 heated wires will be employed to improve the streakline resolution. The CDV ensures automatic and consistent solution replenishment along the entire wire continuously while the tensioning system, illustrated in Fig. 4, maintains a constant strain on the nichrome wires. The tensioner system is equipped with a guitar tuner at the top to set the initial wire tension, while 150 g sinkers are suspended from the lower end to maintain tension as the wire heats and expands during the experiment.
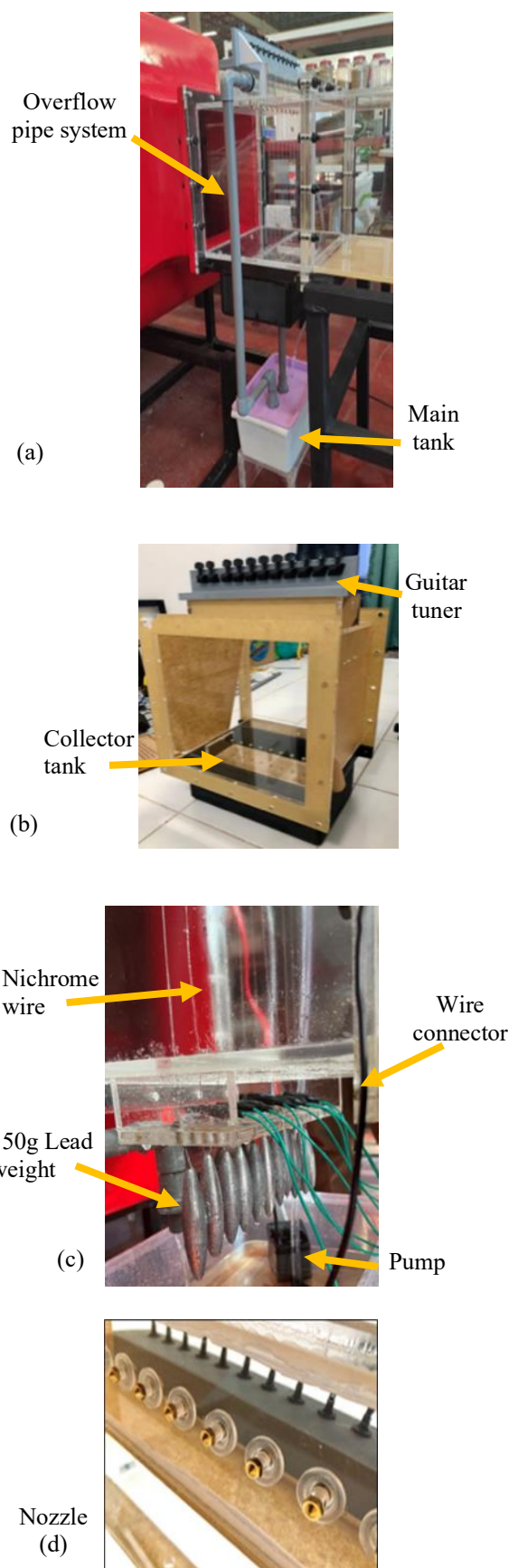

(a)

(b)

(c)

(d)

Fig. 4 Full assembly of the a) CDV, b) CDV tank with tensioner system and reservoir, c) bottom part of the CDV, and d) upper part of the CDV
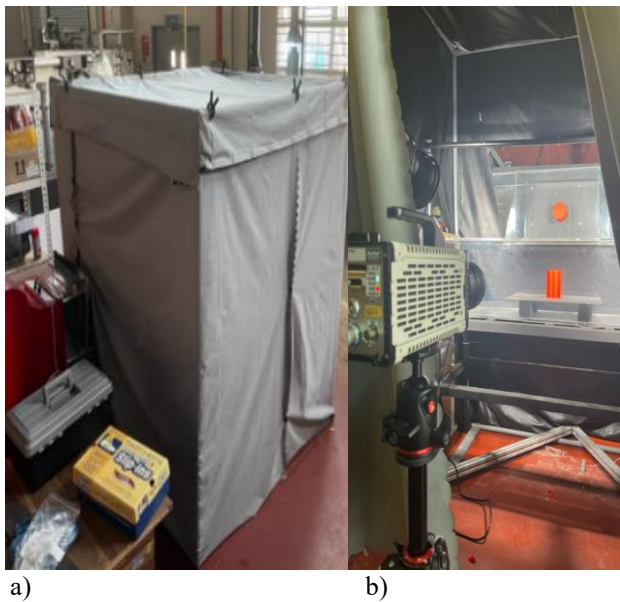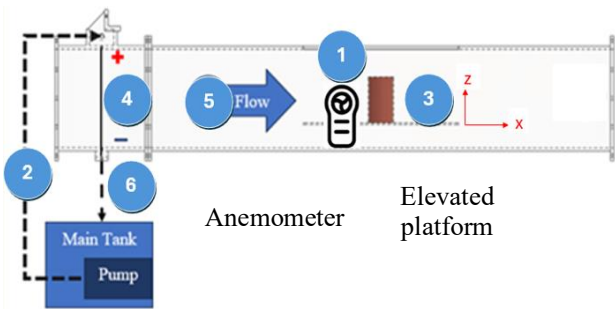
a)   b)

Fig. 5 Studio setup from a) outside and b) inside view with HSC setup

1	Calibration of the fan velocity using an anemometer with an empty tunnel without any model before the experiment. The initial velocity was set at 0.5 m/s.
2.	The water pump was turned on, and the smoke liquid was allowed to fill the tank and flow through the nichrome wire.
3.	The model was placed in the test section at the designated position.
4.	The power input for the nichrome wire was set, and the power supply was turned on.
5.	The nichrome wire heats the smoke liquid, which produces smoke streaklines that are carried through the test section.
6.	Excess smoke fluid flows back into the main tank.

Fig. 6 Diagram for the procedure of the SWT

2.3. Experimental Setup

Figure 5(a) shows the setup of the studio environment enclosed with black curtains to control the lighting conditions and enhance the optical quality of the captured
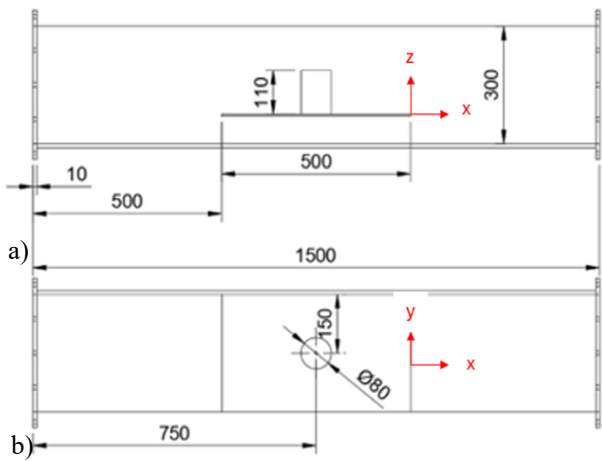

Fig. 7 Schematic figure with dimension (mm) for (a) side and (b) top view of the test section
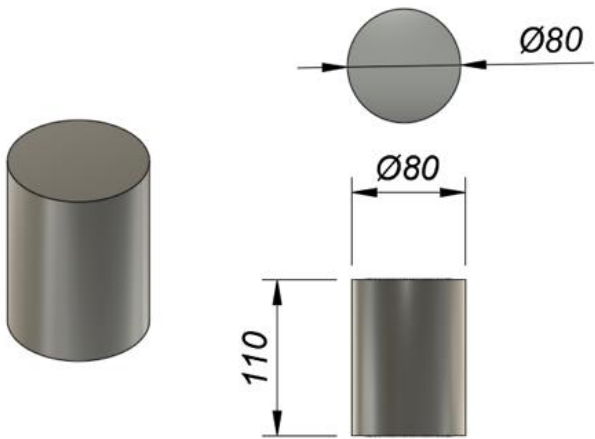

Fig. 8 Surface-mounted finite circular cylinder model with dimension (mm)

images. Illumination was provided by two 300 W photo studio lights. Figure 5(b) shows that the smoke flow velocity was recorded using the MEMRECAM HX-7s high-speed camera, which features an electronic shutter with speeds from 10 ms to 1.1 µs and supports full HD resolution at up to 2000 fps. Figure 6 shows the fully automated experimental setup of the SWT, which utilised Antari Fog Liquid as the smoke solution. A surface-mounted finite circular cylinder model with a diameter of 80 mm and a length of 110 mm, which fulfilled the blockage ratio of below 10 (9.78), as depicted in Fig. 8, was positioned about 750 mm from the smoke wire in the test section, as illustrated in Fig. 7. The background was coated in matte black to enhance the contrast of the smoke streaklines.

2.4. Experimental Cases and Conditions

In the preliminary experiment, the effect of different environmental conditions, such as temperature and humidity, on smoke generation was already considered (Rosminahar et al., 2025; Mat et al., 2023), as the utilized BLWT is an open-loop WT. Smoke production was observed at different times of the day to assess the effects

Table 1 Combination of nozzle size, nichrome wire specification, and wind speed

Nozzle Size (mm)	Nichrome Wire (mm)	Reynolds number (single wire)	Reynolds number (11 wire)	Cross-Sectional Area, A (mm²)	Resistance, R(Ω)	Wind Speed (m/s)	Time Taken (s)
0.3 0.4 0.6 0.8 1.0	0.2	6 to 20	66 to 220	0.0293	2.56E+01	0.5 ~ 1.5	1 ~ 5
	0.4	13 to 38	143 to 418	0.1363	5.50E+00		
	0.5	15 to 42	165 to 462	0.2027	3.70E+00		
	0.6	20 to 58	220 to 638	0.2919	2.57E+00		
	0.8	25 to 77	275 to 840	0.5189	1.45E+00		
	1.0	31 to 95	341 to 1045	0.8107	9.25E-01		

Table 2 Experimental cases

Nozzle size	Nichrome wire diameter	Experimental cases
0.3	0.2	A
0.4	0.2	B
	0.4	C
0.6	0.2	D
	0.4	E
	0.5	F
	0.6	G
0.8	0.2	H
	0.4	I
	0.6	J
	0.8	K
1.0	0.2	L
	0.4	M
	0.6	N
	0.8	O
	1.0	P

of temperature and humidity. No significant differences in smoke generation were noted across these periods from 9 am to 6 pm.

2.4.1. Experiment 1: The Combination of Nozzle Size with Nichrome Wire

The nozzle and nichrome wire diameters played a key role in establishing an optimal ratio that would ensure consistent smoke production and uniform heating. Table 1 presents the possible combinations of nozzle diameter and nichrome wire diameter, with the details of the Reynolds number calculated using the wire diameter and expressed as $Re_d = Uo_d/v$. Both Reynolds numbers are dependent on the surface diameter for the flow during the experiment (Gao & Liu, 2018; Mat et al., 2021a, 2021b), the cross-sectional area, the wire resistance (assuming a wire resistivity [ρ] is 1.50×10^{-6} Ω·m; Serway, 2006), the wind speed, and the duration of smoke production considered in this study. To employ a high-speed camera, a maximum real-time duration of five seconds was considered, which corresponds to 50 s of slow-motion footage. This duration was sufficient to capture continuous smoke generation without interruption, allowing for clear visualisation and analysis of the flow pattern.

The experimental cases are summarised in Table 2, based on various combinations of nozzle size and nichrome wire diameter. The present study examines and discusses the effects of these combinations on the clarity of the generated smoke, specifically focusing on the thickness of the smoke streaklines, the duration and continuity of smoke production, and the uniformity of wire heating.

The visualisation experiment was performed at free-stream velocities Uo of 0.5, 1.0, and 1.5 m/s. This velocity range satisfies the conditions for turbulent flow, making it suitable for the current BLWT experiment. The hydraulic diameter, D_h, was determined as 0.3 m. The critical wind speed for the onset of turbulence, corresponding to a Reynolds number greater than 4000, was calculated as 0.2082 m/s. These velocities correspond to Reynolds numbers for a cylindrical model with a diameter of 80 mm ($Re_D = Uo_D/v$), which range from 2600 to 8000, specifically 2600, 5200, and 8000, as listed in Table 1.

2.4.2. Experiment 2: The Duration of Smoke Generated

Immediately following the completion of the final combination for the nozzle size with nichrome wire, each combination was tested, and the duration of continuous smoke generation in one cycle was recorded. The smoke generation duration was measured by determining the time interval between the initial appearance and the subsidence of the smoke. This was achieved through high-speed video analysis, allowing precise frame-by-frame observation of the smoke behaviour.
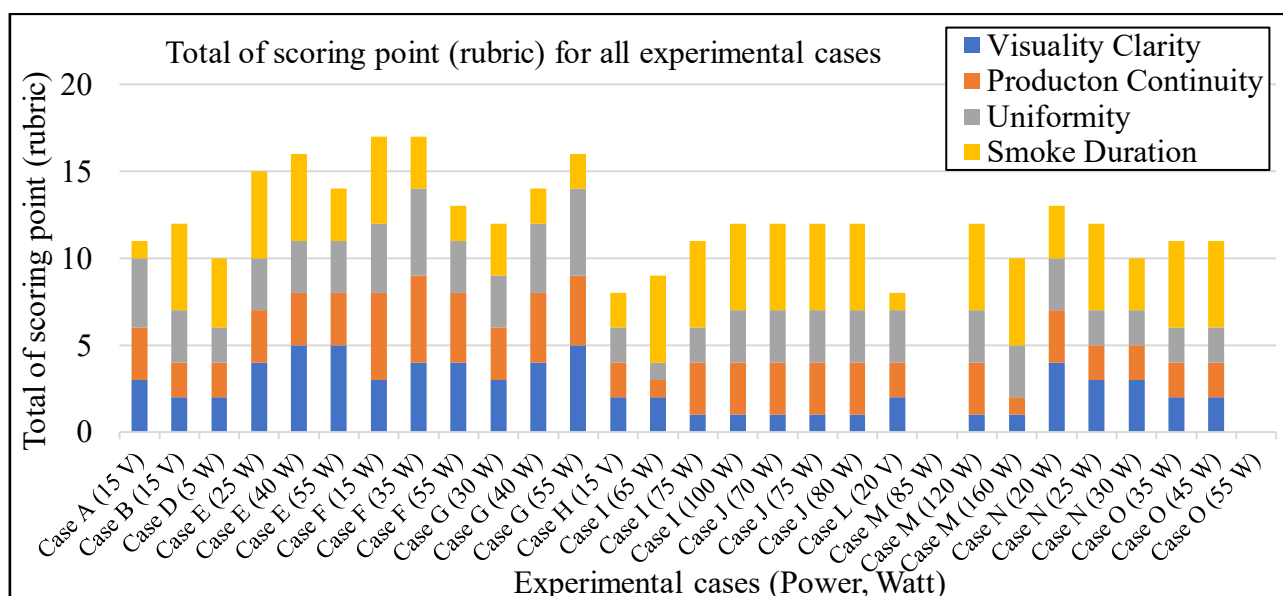
Fig. 9 Stacked column of scoring rubric for smoke generated for all cases at wind speed of 1.5 m/s

2.4.3. Experiment 3: The Impact of Wind Speed on Flow Visualisation

Wind velocity influences the flow rate, turbulence intensity, and development of intricate flow structures. The experiment investigated the impact of wind speed by employing three specific velocities: 0.5, 1.0, and 1.5 m/s. Each wind speed was applied to the previous experiment, and the flow pattern was recorded. The wind speed was measured using an anemometer before the experiment commenced.

3. RESULTS AND DISCUSSION

The effects of varying the nozzle size, nichrome wire diameter, electrical power input (in W), and wind speed on the duration, clarity, and continuity of the smoke streaklines production are summarised in Tables 3 and 5, as well as Fig. 9. Table 3 reports the measured smoke duration for all cases (A until P, each with its corresponding flow rate under a constant duration of 2 min) across the different combinations of power and wind speed. Table 5 presents representative instantaneous images of the smoke generation corresponding to various combinations of nozzle size, nichrome wire diameter, power input, and wind speed. To facilitate a systematic evaluation of the smoke streaklines, Table 5 includes a scoring column based on four primary criteria: visualisation clarity, production continuity, flow uniformity, and smoke duration, as defined in the assessment rubric shown in Table 4 and summarised in Fig. 9.

3.1. Experiment 1: The Combination of Nozzle Size with Nichrome Wire

The combination of nozzle size and wire diameter must allow a balance between resistance, power input, and solution flow rate. A wire diameter that is too small increases resistance and reduces durability, while a wire diameter that is too large lowers resistance but demands excessive power. Similarly, the nozzle size affects the

solution flow rate; a nozzle that is too large results in inadequate vaporisation, whereas a nozzle that is too small restricts the flow of the solution. For example, the current for the 0.2 mm nichrome wire (Cases A, B, D, H, and L) was too low to be accurately measured, allowing only voltage detection (Table 3). This was attributed to the wire's small cross-sectional area, which limits current flow before failure occurs due to overheating, resulting in the wire being burnt entirely. In contrast, the 0.8 mm nichrome wire (Case O) exhibited significantly lower resistance, reducing the heat generation necessary for vaporising the smoke liquid. As a result, higher power input was required.

The results summarised in Table 3 also show that all the wire-nozzle combinations can generate smoke, except when the diameters of the nozzle and wire are identical. In such cases, smoke generation is hindered due to factors such as manufacturing tolerances, metal expansion, and residue buildup. However, an exception was observed in the present work, where the 0.6 mm nozzle and nichrome wire combination (Case G, at 30 W and wind speed ranging from 0.5 to 1.5 m/s) successfully produced smoke despite having matching diameters, with a maximum duration of smoke production ranging from 2.5 to 3 s in real time. However, in Case G, the 30 W-power input generated thinner smoke streaklines of 3 s in real time. Meanwhile, Case G with higher power inputs (40 and 55 W) generated a thicker but shorter duration of smoke streakline of 2 s in real time, as shown in Table 5.

Therefore, initially, the optimal configuration for producing thicker smoke streaklines was set to be Case G with a 0.6 mm nozzle, 0.6 mm nichrome wire, and a 55-W power input, whose overall score was 16 points, as shown in Fig. 9. Since this combination resulted in a very short smoke duration of only 2 s in real time, an additional condition was applied using a 0.6 mm nozzle with a 0.5 mm nichrome wire (Case F) at varying power inputs of 15, 35, and 55 W. Table 5 exhibits how Case F with a 35-W power input performed the best overall. This setup

Table 3 Smoke duration results for cases with combinations of different W power and wind speed

Experimental cases	Power (W)	Flow rate (ml/min)	Wind speed (m/s)	Time taken (s)
A	15 V	1.4	0.5	2
			1	2
			1.5	1
B	15 V	1.7	0.5	3
			1	4
			1.5	5
C	0.4 (Nichrome wire diameter is the same or bigger than the size nozzle)			
D	5	2.5	0.5	4
			1	4
			1.5	4
E	25	0.75	0.5	5
			1	5
			1.5	5
	40		0.5	5
			1	5
			1.5	5
	55		0.5	5
			1	4
			1.5	3
F	15	**0.6**	0.5	3
			1	3
			1.5	5
	35		0.5	2
			1	2
			1.5	**3**
	55		0.5	1
			1	1
			1.5	2
G	30	0.45	0.5	3
			1	3
			1.5	2.5
	40		0.5	2
			1	2
			1.5	2
	55		0.5	1
			1	1.5
			1.5	1.5
H	15 V	11.25	0.5	2
			1	2
			1.5	1.5
I	65	5.2	0.5	5
			1	5
			1.5	5
	75		0.5	5
			1	5
			1.5	5
	100		0.5	5
			1	5
			1.5	5
J	70	5	0.5	5
			1	5
			1.5	5
	75		0.5	5
			1	5
			1.5	5
	80		0.5	5
			1	5
			1.5	5

K	0.8 (Nichrome wire diameter is the same or bigger than the size nozzle)			
L	20 V	28.65	0.5	2
			1	1.5
			1.5	1.5
M	85	23.35	0.5	-
			1	-
			1.5	-
	120		0.5	5
			1	5
			1.5	5
	160		0.5	5
			1	5
			1.5	5
N	20	15	0.5	3.5
			1	5
			1.5	3.5
	25		0.5	4
			1	3.5
			1.5	5
	30		0.5	5
			1	4
			1.5	3
O	35	8.25	0.5	5
			1	5
			1.5	5
	45		0.5	5
			1	5
			1.5	5
	55		0.5	-
			1	-
			1.5	-
P	1.0 (Nichrome wire diameter is the same or bigger than the size nozzle)			

Table 4 Assessment rubric for scoring point

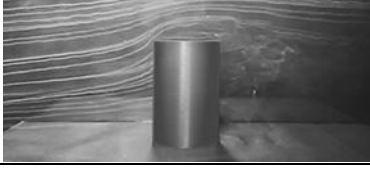|	
P_v = Visualization Clarity	1 (thinnest smoke), 5 (thickest smoke), - (no smoke).
P_c = Production continuity	1 (least persistent), 5 (most persistent), - (no smoke).
P_u = Uniformity	1 (at least uniform), 5 (most uniform), - (no smoke).
P_d = Smoke Duration	1 (10 seconds), 5 (>50 seconds), - (no smoke).
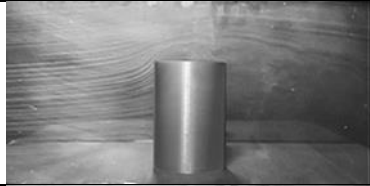
achieved a high total score of 17 points, as shown in the scoring rubric of Fig. 9, reflecting improvements in smoke clarity, production continuity, longer duration, and uniformly heated wire. Based on these results, this combination is considered the optimal condition for generating streaklines using the smoke wire technique in this WT. This combination outperformed the 0.4 and 0.6 mm wires by achieving a stable and well-defined smoke pattern. The resistance of the 0.6 mm nozzle size, coupled with a 0.5 mm nichrome wire diameter and a 35 W power input, enhanced the smoke production's duration and clarity, leading to clearer visualisation.
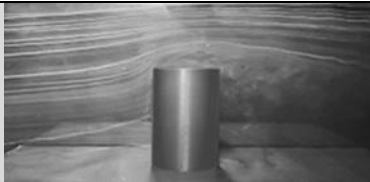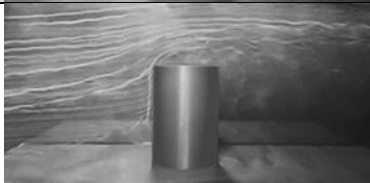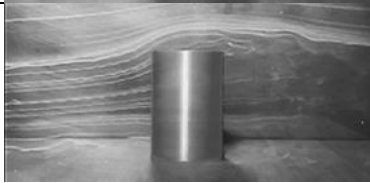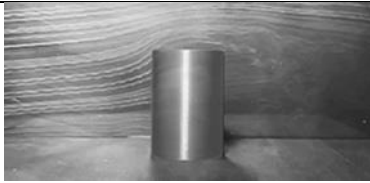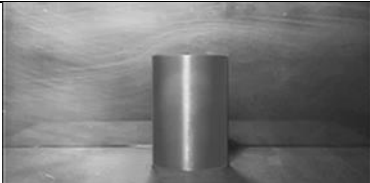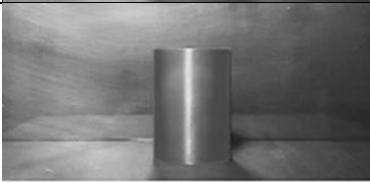
3.2. Experiment 2: The Duration of Smoke Generated
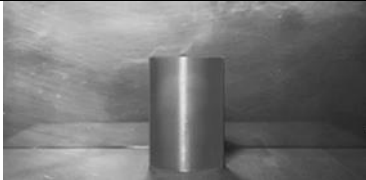
Experiment 2 focused on the duration of the steady-state condition, i.e., a stable, well-defined continuous smoke pattern for all cases. The goal was to determine how long each setup could sustain steady-state smoke production, with a designated upper limit of 5 s in real time, which is equivalent to 50 s in slow-motion high-speed camera footage. This duration is critical and sufficient to obtain the slow-motion footage that could capture the intricate details of the flow patterns.
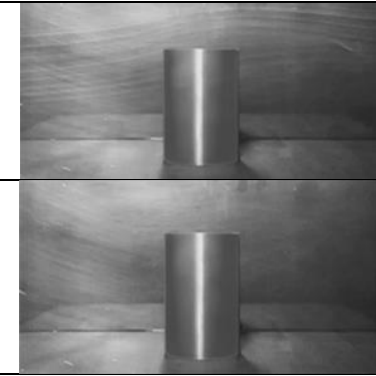
Table 3 depicts how the smoke generation duration varied significantly depending on the nozzle-wire

Table 5 Instantaneous picture for smoke production based on combinations of nozzle size, nichrome wire diameter, power, wind speed with scoring points

Experimental cases	Power (W)	Wind speed (m/s)	Side view	Scoring point (rubric)				
				Pv	Pc	Pu	Pd	Total
A	15 V	1.5		3	3	4	1	11
B	15 V			2	2	3	5	12
D	5			2	2	2	4	10
E	25			4	3	3	5	15
	40			5	3	3	5	16
	55			5	3	3	3	14
F	15	1.5		3	5	4	5	17
	35	0.5		4	4	3	2	13
		1.0		4	4	4	2	14

	75			1	3	3	5	12
	80			1	3	3	5	12
L	20V			2	2	3	1	8
	85			0	0	0	-	0
M	120			1	3	3	5	12
	160	1.5		1	1	3	5	10
	20			4	3	3	3	13
N	25			3	2	2	5	12
	30			3	2	2	3	10
O	35	1.5		2	2	2	5	11

	45				2	2	2	5	11
	55				-	-	-	-	-

combinations and power input. The maximum recorded duration was 5 s in real time, corresponding to the limit set for high-speed camera recordings.

As previously discussed, higher power inputs accelerated liquid evaporation but often resulted in shorter smoke durations due to the limited replenishment rate of the smoke-generating solution. For example, Case G, with a higher power input of 55 W, produced smoke for less than 2 s, whereas lower power inputs yielded durations exceeding 2 s. In this case, the solution flow rate was insufficient to match the rapid evaporation rate, leading to the premature cessation of smoke generation.

In contrast, lower power inputs of 15 and 20 V combined with a 0.2 mm nichrome wire diameter, as in Cases A, H, and L, resulted in insufficient heating. This produced only thin smoke streaklines with very short durations, ranging from 1.0 to 1.5 s. These results highlight the importance of selecting an optimal power range to sustain smoke generation effectively without inducing thermal stress or resulting in inadequate vaporisation.

Table 3 also demonstrates that the combination of nozzle size and nichrome wire diameter must create a balance between the solution flow rate and thermal requirements. A minimal difference between the nozzle and wire diameters restricted the fluid flow, leading to shorter smoke durations. For instance, configurations with identical nozzle and wire sizes, such as in Case G of the 0.6 mm pair, frequently exhibited reduced smoke durations due to limited solution replenishment. In contrast, excessively large differences between the nozzle and wire diameters led to rapid evaporation without sufficient liquid supply, similarly yielding short smoke durations.

In conclusion, Experiment 2 demonstrates that the duration and quality of smoke generation are governed by a complex interplay of nozzle size, nichrome wire diameter, power input, and wind speed. Case F highlights that a 0.1 mm difference between the nozzle and wire diameters, combined with a 35-W power input, provides optimal conditions for sustained, dense, and continuous smoke generation, achieving a total score of 17 points, as shown in Fig. 9. Although the same total score was also recorded for Case F at 15 W, the resulting smoke exhibited slightly lower visual clarity of three points compared to the 35 W configuration of four points. Therefore, this optimal combination facilitates a solution flow rate that matches the evaporation rate, maintaining the necessary thermal balance for high-quality flow visualisation. This evaporation rate represents a potential focus for future work.

3.3. Experiment 3: The Impact of Wind Speed on Flow Visualisation

Experiment 3 focuses on the influence of wind speed on the quality, continuity, and clarity of smoke streaklines in this SWT flow visualisation method. Wind speed has been identified as a critical factor affecting streakline formation and stability. The present study investigated the effects of three wind speed conditions— 0.5, 1.0, and 1.5 m/s—on smoke streakline behaviour, based on the data presented in Tables 3 and 5.

Tables 3 and 5 show that at a minimum velocity of 0.5 m/s, the smoke exhibited a dense formation. However, its distribution was uneven, primarily accumulating at the upper region of the test section. This led to the formation of thick, streaky patterns exhibiting restricted vertical uniformity. The reduced velocity facilitated the persistence of smoke particles, resulting in an uneven distribution and hindering the clear visualisation of flow patterns.

At 1.0 m/s, the smoke distribution is improved, with thickness becoming more uniform and fewer streaks observed. However, occasional waves still appeared, suggesting intermittent disruptions in smoke flow. This indicated that although 1.0 m/s allowed better dispersion than 0.5 m/s, the airflow was still insufficient to maintain fully stable and continuous streaklines.

Meanwhile, the best performance was observed at 1.5 m/s. The smoke streaklines were straight, continuous, and vertically uniform, making them ideal for visualisation. The increased velocity enhanced smoke dispersion, preventing accumulation and ensuring consistent flow across the test section. This wind speed provided the most stable flow conditions for capturing detailed flow patterns. Table 5 summarises both the top and side views of the flow pattern for this condition of 1.5 m/s wind speed.

The data presented in Tables 3 and 5 demonstrate that optimal smoke visualisation is contingent upon the interaction of wind speed, power input, and nozzle-wire combinations. Case F, operating at 35 W, consistently yielded the most stable, continuous, and vertically uniform smoke streaklines across varying wind speeds, with optimal results observed at 1.5 m/s.
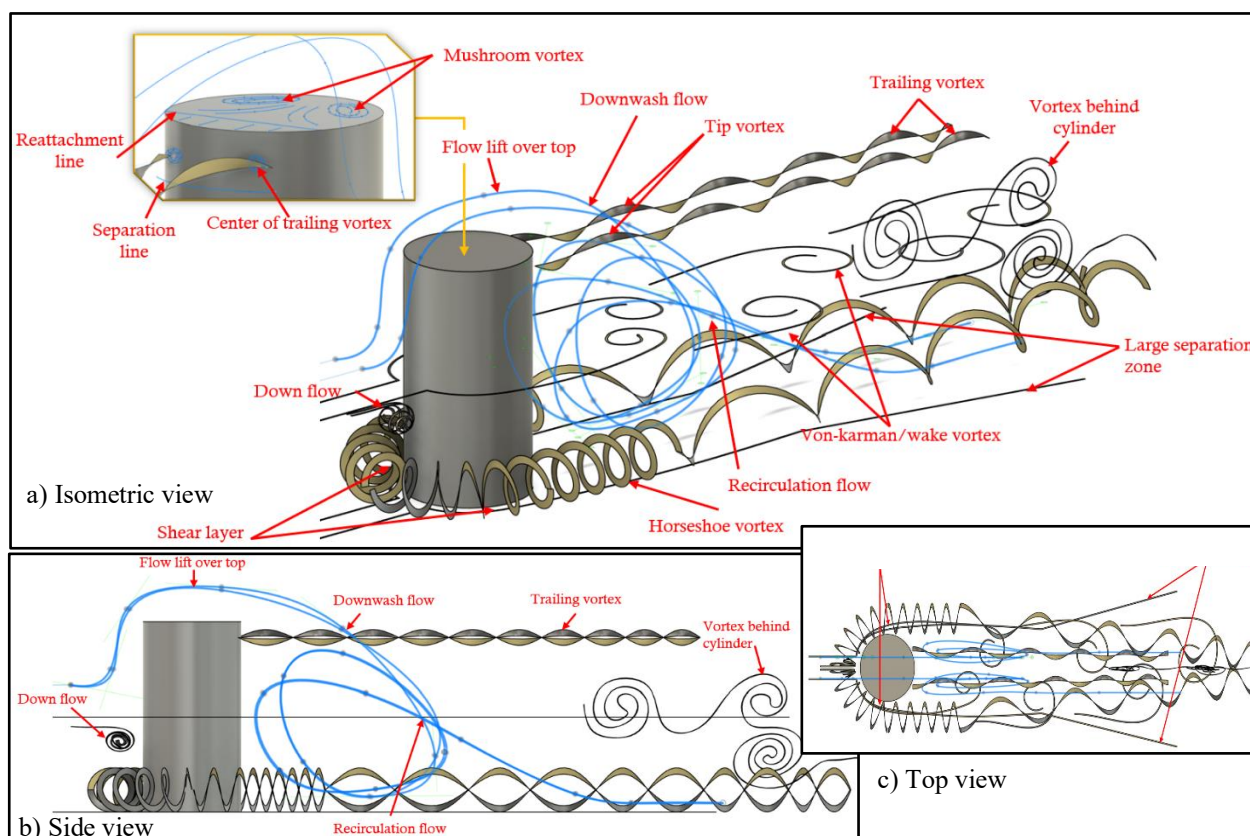
Fig. 10 Flow structures typically found around a finite circular cylinder from literature review

Table 3 also reveals that wind speed influenced the duration of continuous smoke generation. At lower wind speeds, the smoke duration was shorter due to the uneven dispersion and accumulation of smoke. At 1.5 m/s, the optimal Case F at 35 and 15 W maintained a 3 s and 5 s smoke generation duration, demonstrating that this setup balanced solution flow and vaporisation rates even at higher velocities. This combination ensures optimal visualisation conditions by balancing the power input, solution flow, and thermal stability.

Table 5 highlights that at a higher velocity, 1.5 m/s, the results were related to the clarity of smoke production, specifically the thickness of the generated smoke streaklines, as well as the duration of smoke production. The table shows that smoke clarity decreased when mixing occurred during the experiment. For example, in the optimal configuration of Case F (0.6 mm nozzle size and 0.5 mm wire diameter), a decline in smoke clarity was observed with decreasing wind speed. At a wind speed of 1.5 m/s, the configuration achieved a score of 17 points, whereas at 0.5 m/s, the score decreased to 13 points. This reduction reflects diminished smoke streakline definition under slower flow conditions, likely due to reduced momentum and less effective entrainment of the smoke into the airstream.

3.4. Summary of Combinations on Experimental Conditions (Experiments 1, 2 & 3).

Figure 9 displays the scoring rubric results by comparing the smoke produced by different combinations of nozzle size and wire diameter. Different power inputs

are also included in Table 3 to validate the best combination of the variance. The data from the stacked column proved the best combination for the nozzle size, with a wire diameter of 0.6 mm as the nozzle size and a 0.5 mm nichrome wire diameter.

Comparison of flow patterns from present work with the existing flow patterns from literature

The smoke generation validity under the selected optimal conditions was supported by comparing the observed flow patterns with those obtained in previous experiments and documented in the literature. Figure 10 shows the summary of the flow pattern or flow structure around the mounted circular cylinder obtained in previous literature (Cornaro et al., 1999; Sumner, 2013; Ferradosa et al. 2014; He et al., 2017; Dol et al., 2021; Welzel, 2021; Cho et al., 2022; Liu et al., 2023). Additionally, Fig. 10 reveals that the flow pattern around the mounted circular cylinder includes a mushroom vortex, the centre of a trailing vortex, a downflow, a downwash flow, flow lift over the top surface, recirculation zones, a horseshoe vortex, vortex shedding behind the cylinder, a tip vortex, a trailing vortex, a von-karman or wake vortex, shear layers, and a large separation zone. As previously mentioned, the present study, as illustrated in Fig. 11, successfully captured most of the flow structures around the mounted circular cylinder, with the exception of the horseshoe vortices and shear layers. This limitation was primarily due to the camera positioning, which was not optimised or specifically configured to capture these regions; this is an area identified for improvement in future experimental setups.

a)   b)
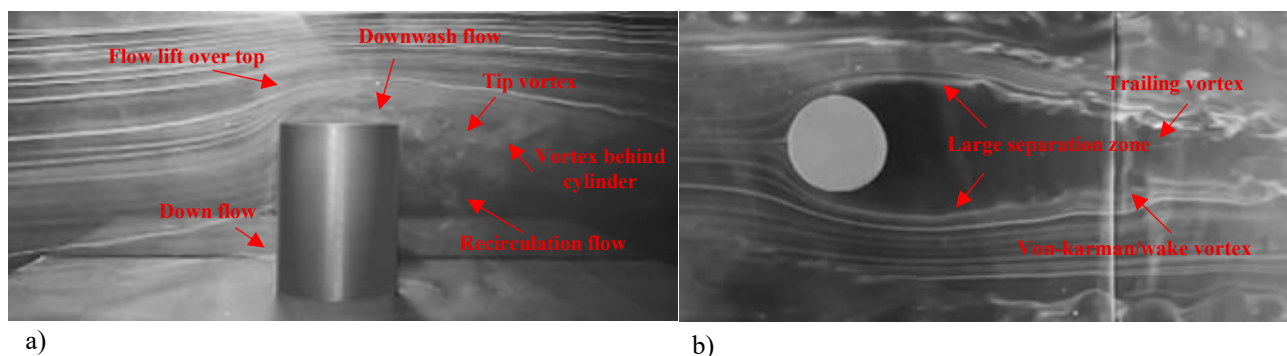
Fig. 11 An instantaneous picture of (a) side view, and (b) top view of the finite circular cylinder in the optimal condition of the SWT, Case F (0.6 mm nozzle size and 0.5 mm wire diameter) at 1.5 m/s

The side view (Fig. 11 a) clearly reveals several key flow features, including an upward-lifting flow over the model, a localised downflow at the frontal lower region, a downwash, tip vortices, and a trailing vortex behind the cylinder. Meanwhile, the top view (Fig. 11 b) highlights a prominent separation region and the presence of wake vortices extending downstream in the wind tunnel. Certain flow structures—such as the reattachment line, separation line, and mushroom vortex—could only be inferred through references in the literature and numerical simulations as they were not directly observable via the visualisation techniques used in this study.

In summary, the present work demonstrates that precise calibration of the nozzle size, wire diameter, and power input is essential for optimal smoke wire technique performance. The identified optimal combination serves as a reference for future experiments involving multiple wires and complex flow patterns, ensuring clear, continuous, and stable smoke visualisation.

4. CONCLUSION

The results from Experiment 1 indicated that the nichrome wire diameter should generally be slightly smaller than the nozzle size to accommodate varying tolerances across different configurations. An exception was observed with the 0.6 mm nozzle, where a larger wire diameter was still effective.

In Experiment 2, which recorded the duration of smoke generation, continuous smoke production was typically sustained for 3 s to 5 s in real time. This corresponds to approximately 30 s to 50 s when viewed in slow-motion footage captured by a high-speed camera. In conclusion, higher W power results in a thicker but shorter duration of smoke production. This result reflects the scoring rubric in Table 3, which yielded the highest score, 17 points. A 35-W power condition was recorded as the moderate power range that generated vertically informed and continuous streaklines in 30 s of slow-motion footage.

In Experiment 3, a wind speed of 1.5 m/s was determined as optimal for the visualisation experiment, facilitating clear and continuous flow patterns. Therefore, the optimum experimental conditions for the smoke wire technique in the BLWT at UMPSA were recorded to be a 0.6 mm nozzle size, a 0.5 mm nichrome wire diameter, 35 W power, and 1.5 m/s wind speed.

To conclude, some of the difficulties encountered during the experiment arose from the inconsistent thickness of the smoke during mixing. As the experiment progressed, the smoke became thinner, indicating that mixing disrupted the stability of smoke generation. This suggests that even minor discrepancies in the flow system, particularly in the flow rate influenced by the combination of nozzle size and wire diameter, could allow the smoke solution to be initially generated but fail to sustain it. This was likely due to uneven heating of the nichrome wire along its length, leading to reduced or unstable smoke production. This poses a challenge for achieving reliable flow pattern visualisation.

To effectively scale the system for larger or more complex experimental setups, a combination of mechanical enhancements and procedural improvements is necessary. Implementing features such as an automatic timer, an adjustable turntable, and a precisely positioned compact SWT system could significantly enhance the data consistency, visualisation flexibility, and focus on critical areas. Additionally, replacing manual smoke generation controls with a peristaltic pump would enable greater accuracy and adaptability in flow visualisation, making the system more robust and suitable for diverse applications.

CONFLICT OF INTEREST

The authors declare that there are no conflicts of interest to report.

AUTHORS CONTRIBUTION

Nurizzatul Atikha Binti Rahmat: Conceptualization, Data curation, Funding acquisition, Methodology, Project Administration, Resources, Supervision, Writing – original draft. **Achmad Rizal:** Data curation, Formal analysis, Investigation, Methodology, Visualization Writing – original draft. **Kamil Khalili:** Data curation, Formal analysis, Investigation, Methodology,

REFERENCES

Abdullah, K. K. Rahmat, N. A. & Khairunizam, K. A. (2022). Flow pattern around traditional Malay house using enhanced smoke wire technique in a boundary layer wind tunnel, *Engineering Technology International Conference (ETIC 2022)*, Online Conference, Kuantan, Malaysia, 2022, pp. 49-56, https://doi.org/10.1049/icp.2022.2569.

Azizi, M. N. (2012). *Design and Construction of smoke wire apparatus for wind tunnel flow visualization*. http://utpedia.utp.edu.my/id/eprint/5562

Barlas, E., Buckingham, S., & van Beeck, J. (2016). Roughness effects on wind-turbine wake dynamics in a boundary-layer wind tunnel. *Boundary-Layer Meteorology, 158*(1), 27–42. https://doi.org/10.1007/s10546-015-0083-z

Barlow, J. B., Rae, W. H., & Pope, A. (1999). *Low-speed wind tunnel testing*. Wiley.

Batill, S. M., & Mueller, T. J. (1981). Visualization of transition in the flow over an airfoil using the smoke-wire technique. *AIAA Journal, 19*(3), 340–345. https://doi.org/10.2514/3.50953

Bradshaw, P. (1966). The effect of wind-tunnel screens on nominally two-dimensional boundary layers. *Journal of Fluid Mechanics, 22*(4), 679–687. https://doi.org/10.1017/S0022112065001064

Cermak, J. E., Cochran, L. S., & Leflier, R. D. (1995). Wind-tunnel modelling of the atmospheric surface layer. *Journal of Wind Engineering and Industrial Aerodynamics, 54–55*(C), 505–513. https://doi.org/10.1016/0167-6105(94)00065-L

Cho, H. W., Park, Y. G., Ha, M. Y., & Seo, Y. M. (2022). Three-dimensional mixed convection in a rectangular enclosure containing a circular cylinder. *Heat Transfer Engineering, 43*(11), 879–895. https://doi.org/10.1080/01457632.2021.1919970

Cook, N. J. (1975). A boundary layer wind tunnel for building aerodynamics. *journal of Industrial Aerodynamics, 1*.

Cornaro, C., Fleischer, A. S., & Goldstein, R. J. (1999). Flow visualization of a round jet impinging on cylindrical surfaces. www.elsevier.nl/locate/etfs

Dol, S. S., Mohd, A. M., Khairun, M., Iskandar, B. S. (2006). *An Improved Smoke-Wire Flow Visualization Technique*. https://api.semanticscholar.org/CorpusID:13905908

Dol, S. S., Yong, T. H., Chan, H. Bin, Wee, S. K., & Sulaiman, S. A. (2021). Turbulence characteristics of the flexible circular cylinder agitator. *Fluids, 6*(7). https://doi.org/10.3390/fluids6070238

Ferradosa, T., Pinto, F. T., Oliveira, B., Simons, R., & Porter, K. (2014). *Scour around marine foundations in layered sediments: a mathematical modelling approach*. https://www.researchgate.net/publication/261510986

Fitriady, M. A., Rahmat, N. A., & Mohammad, A. F. (2022). Numerical simulation on the elucidation of wake flow structure behind a single quarter elliptic-wedge spire. *Engineering Technology International Conference (ETIC 2022), 2022*, 289–297. https://doi.org/10.1049/icp.2022.2627

Fitriady, M. A., Rahmat, N. A., & Mohammad, A. F. (2023a). *Urban heat island phenomenon in tropical countries: analysis of the wake flow behind slender high-rise building.* Lecture Notes in Energy (Vol. 92, pp. 273–288). Springer Science and Business Media Deutschland GmbH. https://doi.org/10.1007/978-981-19-6688-0_17

Fitriady, M. A., Rahmat, N. A., & Mohammad, A. F. (2023b). Vertical and spanwise wake flow structures of a single spire over smooth wall surface in a wind tunnel. *Journal of Applied Fluid Mechanics, 16*(12), 2459–2470. https://doi.org/10.47176/jafm.16.12.1890

Fitriady, M. A., Rahmat, N. A., Mohammad, A. F., & Zaki, S. A. (2023c). Numerical simulation of the boundary layer development behind a single quarter elliptic-wedge spire. *Journal of Mechanical Engineering and Sciences,* 9421–9432. https://doi.org/10.15282/jmes.17.2.2023.1.0745

Fitriady, M. A., Rahmat, N. A., Mohammad, A. F., & Zaki, S. A. (2023d). Effect of mesh refinement on vertical and lateral velocity profiles of the wake flow behind a spire using computational fluid dynamic (CFD). *Journal of Engineering and Technology 14*(2), 2180–3811. https://jet.utem.edu.my/jet/index

Fu, J. Y., Li, Q. S., Wu, J. R., Xiao, Y. Q., & Song, L. L. (2008). Field measurements of boundary layer wind characteristics and wind-induced responses of super-tall buildings. *Journal of Wind Engineering and Industrial Aerodynamics, 96*(8–9), 1332–1358. https://doi.org/10.1016/j.jweia.2008.03.004

Gao, N., & Liu, X. H. (2018). An improved smoke-wire flow visualization technique using capacitor as power source. *Theoretical and Applied Mechanics Letters, 8*(6), 378–383. https://doi.org/10.1016/j.taml.2018.06.010

Hadi Wijaya, M., Ahmad Zaki, S., Faiz Mohamad, A., Atikha Rahmat, N., Othman, A., Malaysia, T., Sultan Yahya Petra, J., & Lumpur, K. (2024). *Investigation of wind flow characteristics using passive devices in boundary layer wind tunnel*. Nurizzatul Atikha Rahmat & Nor'azizi Othman (Vol. 11, Issue 1). www.jtse.utm.my

He, G. S., Wang, J. J., Pan, C., Feng, L. H., Gao, Q., & Rinoshika, A. (2017). Vortex dynamics for flow over a circular cylinder in proximity to a wall. *Journal of*

Fluid Mechanics, 812, 698–720. https://doi.org/10.1017/jfm.2016.812

Hohman, T. C., Van Buren, T., Martinelli, L., & Smits, A. J. (2015). Generating an artificially thickened boundary layer to simulate the neutral atmospheric boundary layer. *Journal of Wind Engineering and Industrial Aerodynamics, 145*, 1–16. https://doi.org/10.1016/j.jweia.2015.05.012

Ismail, A. T., & Kamaruddin, N. M. (2020). *Development of a flow visualization technique in wind tunnel for hydrokinetic turbine application*. IOP Conference Series: Materials Science and Engineering, 920(1). https://doi.org/10.1088/1757-899X/920/1/012034

Isyumov, N. (1967). The application of the boundary layer wind tunnel to the prediction of wind loading. https://www.researchgate.net/publication/285121067

Kareem, A. A., Abbas, M. K., & Khammas, F. A. (2021). *Aerodynamic study of low-speed wind tunnel contraction section: design and manufacturing.* IOP Conference Series: Materials Science and Engineering, 1094(1), 012077. https://doi.org/10.1088/1757-899x/1094/1/012077

Kulkarni, V., Sahoo, N., & Chavan, S. D. (2011). Simulation of honeycomb-screen combinations for turbulence management in a subsonic wind tunnel. *Journal of Wind Engineering and Industrial Aerodynamics, 99*(1), 37–45. https://doi.org/10.1016/j.jweia.2010.10.006

Kumaraswamy, T., Bharawaj, V. V. S. N., Garre, P. (2014). Design and Analysis of Transonic Wind Tunnel. *Global Journal of Researches in Engineering, 14*(1). https://globaljournals.org/GJRE_Volume14/1-Design-and-Analysis.pdf

Li, X., & Li, Q. S. (2019). Observations of typhoon effects on a high-rise building and verification of wind tunnel predictions. *Journal of Wind Engineering and Industrial Aerodynamics, 184,* 174–184. https://doi.org/10.1016/j.jweia.2018.11.026

Liu, Y., Cheng, B., & Deng, X. (2013). An application of smoke-wire visualization on a hovering insect wing. *Journal of Visualization, 16*(3), 185–187. https://doi.org/10.1007/s12650-013-0165-2

Liu, Y., Liu, J., & Gao, F. P. (2023). Strouhal number for boundary shear flow past a circular cylinder in the subcritical flow regime. *Ocean Engineering, 269*. https://doi.org/10.1016/j.oceaneng.2022.113574

Mat, M. N. H., Mohd-Ghazali, N., Shamsuddin, H. S. & Estelle, P. (2023). Thermofluid behaviour of boron nitride nanotube nanofluid in a microchannel under optimized conditions. *Journal of Thermal Analysis and Calorimetry 148*, 3035–3044. https://doi.org/10.1007/s10973-022-11472-8

Mat, M. N. H., Nasir, M. F. M., Asmuin, N. Z. (2021a). Response Surface Analysis of DIB Nozzle Geometry on Acoustic Power Level using Central Composite Design of Experiment. *Journal of Physics:*

Conference Series. 2129 012019. http://doi.org/10.1088/1742-6596/2129/1/012019

Mat, M. N. H., Nasir, M. F. M., Sies, M. F. (2021b). Velocity Flow Field Characteristic on Nozzle Cavity using Central Composite Design of Computational Method for Dry Ice Blasting System. *Journal of Physics: Conference Series* 2129 012020. http://doi.org/10.1088/1742-6596/2129/1/012020

Mathur, N. B., Ramesh, G., & Yajnik, K. S. (1988). Continuous coloured smoxe-wire technique for flow visualisation.

Mehta, R. C. (2021). Numerical simulation of shock wave turbulent boundary layer interaction over flat plate at Mach 6. *Journal of The Institution of Engineers (India): Series C.* https://doi.org/10.1007/s40032-021-00732-5

Mehta, R. D., & Bradshaw, P. (1979). Design rules for small low speed wind tunnels. *Aeronautical Journal, 83*(827), 443–449. https://doi.org/10.1017/s0001924000031985

Niemann, H. J. (1993). The boundary layer wind tunnel: an experimental tool in building aerodynamics and environmental engineering. *Journal of Wind Engineering and Industrial Aerodynamics, 48.*

Rahmat, N. A., Hagishima, A., Ikegaya, N., & Tanimoto, J. (2016). *An experimental study on aerodynamic interaction between a boundary layer generated by a smooth and rough wall and a wake behind a spire.* Kyushu University Interdisciplinary Graduate School of Engineering Sciences Version: Rights: Kyushu University Interdisciplinary Graduate School of Engineering Sciences Report, 37(2), 19–26. https://doi.org/10.15017/1560669

Rahmat, N. A., Hagishima, A., Ikegaya, N., & Tanimoto, J. (2018). Experimental study on effect of spires on the lateral nonuniformity of mean flow in a wind tunnel. *Evergreen, 5*(1), 1–15. https://doi.org/10.5109/1929670

Rahmat, N. A., Haji Abdullah, K.K., Khairunizam, K.A. (2023a). Natural Ventilation in Traditional Malay House: A Study of Flow Pattern by an Enhanced Smoke Wire Technique. In: Sulaiman, S.A. (eds) Energy and Environment in the Tropics. Lecture Notes in Energy, vol 92. Springer, Singapore. https://doi.org/10.1007/978-981-19-6688-0_18

Rahmat, N. A., Ramli, M. R., Hassan, M. H. C., Abdullah, K. K. H., & Khairunizam, K. A. (2023b). *Enhanced smoke wire technique with control dripping valve in a small scaled quasi-atmospheric boundary layer wind tunnel*. Lecture Notes in Mechanical Engineering, 611–627. https://doi.org/10.1007/978-981-19-14577_47

Rosminahar, S. N, Mat, M. N. H., & M. Yusup, E. (2024). Mesh Refinement for Dynamics Airflow in Health Care. *International Journal of Integrated Engineering, 16*(6), 90-99. https://penerbit.uthm.edu.my/ojs/index.php/ijie/article/view/17399

Rosminahar, S. N., Mat, M. N. H., Rani, M. F. H., Wong Keng, Y., & Akrami, M. (2025). Influence of Air Changes Per Hours (ACH) on Human Thermal Comfort under Stratum Ventilation Setting in a Single Isolated Wardroom. *Journal of Advanced Research in Fluid Mechanics and Thermal Sciences, 130*(2), 90–99. https://doi.org/10.37934/arfmts.130.2.9099

Schneider, S. P. (2003). Development of Quiet-Flow Supersonic Wind Tunnels for Laminar-Turbulent Transition Research: Final Report for NASA Langley Grant NAG-1-1133. https://apps.dtic.mil/sti/pdfs/ADA640235.pdf

Serrano-Aguilera, J. J., García-Ortiz, J. H., Gallardo-Claros, A., Parras, L., & del Pino, C. (2016). Experimental characterization of wingtip vortices in the near field using smoke flow visualizations. *Experiments in Fluids, 57*(8). https://doi.org/10.1007/s00348-016-2222-9

Settles, G. (1986). Modern development in flow visualization. *Aiaa Journal - AIAA J. 24*. 1313-1323. https://doi.org/10.2514/3.9437

Serway, R. A. (2006). *College physics* (Vol. 2). Brooks/Cole, Thomson Learning.

Soria, J., Chiu, W. K., & Norton, M. P. (1990). A study of unsteady laminar boundary layer flow on a flat plate using a smoke-wire/silhoutte flow visualization technique, Experimental Thermal and Fluid Science, 3(3), 291-304. https://doi.org/10.1016/0894-1777(90)90004-Q.

Sumner, D. (2013). Flow above the free end of a surface-mounted finite-height circular cylinder: A review. *Journal of Fluids and Structures, 43*, 41–63. https://doi.org/10.1016/j.jfluidstructs.2013.08.007

Trinder, M., & Jabbal, M. (2013). Development of a smoke visualisation system for wind tunnel laboratory experiments. *International Journal of Mechanical Engineering Education, 41*(1), 27–43. https://doi.org/10.7227/IJMEE.41.1.5

Vikneshvaran, Zaki, S. A., Rahmat, N. A., Ali, M. S. M., & Yakub, F. (2020). Evaluation of atmospheric boundary layer in open-loop boundary layer wind tunnel experiment. *Journal of Advanced Research in Fluid Mechanics and Thermal Sciences, 72*(72), 79–92. https://doi.org/10.37934/ARFMTS.72.2.7992

Wang, J., Foley, S., Nanos, E. M., Yu, T., Campagnolo, F., Bottasso, C. L., Zanotti, A., & Croce, A. (2017). Numerical and experimental study of wake redirection techniques in a boundary layer wind tunnel. *Journal of Physics: Conference Series, 854*(1). https://doi.org/10.1088/1742-6596/854/1/012048

Welsh, A. (2013). Low turbulence wind tunnel design and wind turbine wake characterization recommended citation. https://dc.uwm.edu/etd/180

Welzel, M. (2021). Wave-current-induced scouring processes around complex offshore structures. https://doi.org/10.15488/11225

Wu, T. J. (1992). Visualization of Stall Characteristics of Airfoils Using the Smoke-Wire Technique. https://arc.uta.edu/publications/td_files/T-J%20Wu.pdf

Yarusevych, S., Sullivan, P. E., & Kawall, J. G. (2009). Smoke-wire flow visualization in separated flows at relatively high velocities. *AIAA Journal, 47*(6), 1592–1595. https://doi.org/10.2514/1.43539

Yi, W., Zhou, P., Fang, Y., Guo, J., Zhong, S., Zhang, X., Huang, X., Zhou, G., & Chen, B. (2021). Design and characterization of a multifunctional low-speed anechoic wind tunnel at HKUST. *Aerospace Science and Technology, 115*. https://doi.org/10.1016/j.ast.2021.106814